

Operational experience and performance of the CMS pixel detector during the first LHC beams

Valeria Radicci for the CMS Collaboration

The University of Kansas, Lawrence, Kansas 66045, US

DOI: <http://dx.doi.org/10.3204/DESY-PROC-2010-01/194>

The CMS pixel detector is a complex system consisting of 66M pixels of $100 \times 150 \mu\text{m}$ size with the main goal of high resolution reconstruction of charged particle tracks. It took almost 10 years of design, construction and commissioning before operation with LHC beams. After the installation in July 2008, the pixel detector was commissioned and calibrated with cosmic muons and the first proton collisions. This paper describes the operational experience, the calibration, and the performance of the pixel detector.

1 Introduction

The silicon pixel tracker is the core of CMS and the closest detector to the interaction point. It is a complex system with 66M pixel channels covering an area of approximately 1 m^2 designed to provide three high precision hits for charged particle tracks in the CMS 3.8 T magnetic field [1].

After 10 years of design and construction it was inserted in CMS in July 2008, and then calibrated and commissioned for more than one year with cosmic muons while awaiting beams. This long period of cosmic runs was useful for the detector understanding and calibration. The cosmic data were used for setting the operating parameters as well as for the time and space alignment [2], [3]. In fall 2009 the operation with colliding beams started, these data were used to complete the calibration procedure and to evaluate the detector performance.

In this paper the results obtained with p-p collisions at center-of-mass energies of 0.9, 2.3, and 7 TeV are shown. A short introduction of the pixel system and operating conditions is given at the beginning, then the status of the present detector is discussed. The calibration and commissioning phases are presented: timing calibration, threshold optimization, bias scan, and Lorentz angle measurement. In the final section, the pixel detector performance with first beams is shown focusing on comparison of data and Monte Carlo, hit detection efficiency, and hit resolution measurements.

2 The CMS pixel detector status

The silicon pixel detector consists of three barrel layers with radii of 4.4, 7.3, 10.2 cm, respectively, and two end-cap disks placed on each side of the barrel at a distance in z of 35.5 and 48.5 cm from the interaction point, respectively.

The basic element of the detector is a module composed of a silicon pixel sensor bump-bonded to a readout chip (PSI-46 ROC) placed on carbon fiber supports. The 4160 pixel cells

of the ROC are arranged in a 52 column and 80 row matrix. In each cell the charge produced in the sensor is amplified, formed, and compared to a threshold. The charge over the threshold, together with a time stamp, is stored in a buffer at the ROC periphery waiting for the accepted LHC level 1 trigger [4]. The technology chosen for the silicon sensor is $n+$, $100 \times 150 \mu\text{m}$ pixels on n substrate. Slightly different sensor thicknesses and pixel isolation techniques are used: $285 \mu\text{m}$ p-spray for the barrel and $270 \mu\text{m}$ p-stops for the end caps [5].

During data taking with beams the operating conditions are not changed from the cosmic runs in order to take advantage of the calibration already performed. The coolant temperature is at 7.4°C ¹ and the bias voltage is 150 V in the barrel and 300 V in the end caps.

Currently 98.3% of the pixel detector is in operation: 98.9% of the barrel and 96.8% of the endcaps. The main reasons for failures are broken wire bonds or missing high voltage connections. The number of dead pixels is very low: less than 0.02% in the barrel and less than 0.1% in the endcaps, consistent with the observation during the module test. The number of noisy pixels is negligible, the total fraction is less than 5×10^{-6} [2].

3 Detector calibration

Before operating the system each component of the analog readout chain has to be adjusted: the ROC, the analog optical hybrid and the front end opto-receiver. The optimization procedure is repeated for each channel using an internal calibration signal (V_{cal}) created by the ROC at the pixel preamplifier input [2].

An important calibration to be performed is the optimization of the comparator thresholds. The particle position reconstruction in the pixel detector relies not only on the charge measured by a single pixel but also on the charge shared between pixels and the analog interpolation of the charge between neighboring channels. In order to improve the spatial resolution, the pixel detector has to be sensitive to smaller charges and the pixel charge response has to be uniform. For this purpose an iterative procedure is implemented to lower the ROC threshold to find the minimum value at which the pixels are still 100% efficient. Trim bits at the comparator are also tuned to reduce the pixel to pixel threshold variations. In Figure 1(a), the distribution of the final thresholds is shown, the mean value is 2457. Due to time walk, small signals can take more than a bunch crossing to fire the comparator, and can be associated with a wrong bunch crossing. The minimum hit signal that fires the discriminator threshold in time with the trigger bunch crossing is higher than the absolute threshold and can be estimated comparing the observed cluster size with that expected from MC. The minimum charge that can be correctly readout is approximately $3200 e^-$.

Another calibration performed is the timing alignment. The CMS clock must arrive at the correct time for the 25 ns window to be associated correctly to the signal produced by the particles. The best delay maximizes the cluster charge, size, and detection efficiency. A first timing alignment was performed using the fiber lengths. Later, a coarse scan was performed measuring the cluster charge and size with early beams and an accurate timing optimization was achieved measuring the efficiency with beams at 7 TeV.

The high voltage bias scan was also performed with beams at 7 TeV. In Figure 1(b), the efficiency measured in the barrel as a function of bias voltage is shown. At the operating point, 150 V, the efficiency is over 99% and the detector is over depleted. The efficiency curve is

¹The sensor temperature is around the coolant temperature plus 6°C .

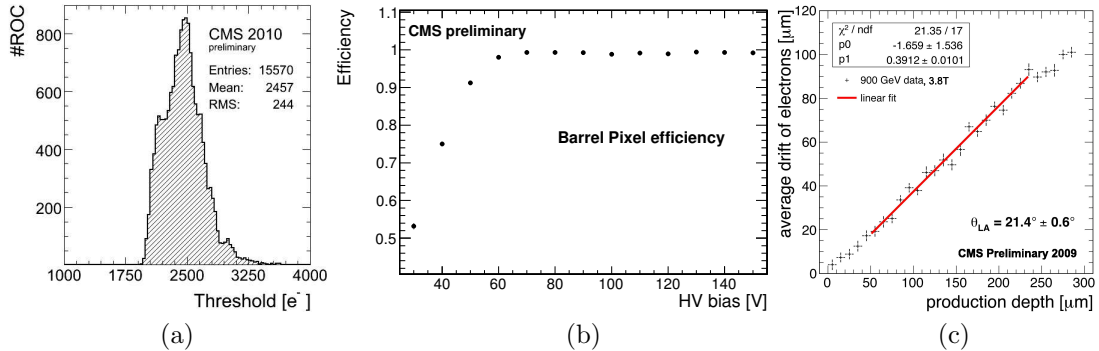


Figure 1: (a) Distribution of the thresholds in barrel and end caps; (b) detector efficiency vs bias voltage in the barrel; (c) Lorentz angle measurement with the *grazing angle method*.

expected to change in the future due to aging and radiation effects and will be continually re-measured to monitor the operating voltage.

The charge sharing is enhanced in the magnetic field by the Lorentz force on the charge deposited by ionization. The Lorentz angle (θ_{LA}) has to be measured to correct the hit position. Two methods are used to measure θ_{LA} . The *minimum cluster size* method, more suited to use with cosmic data, measures the cluster size as a function of the track angle. The minimum size is observed when the charges are produced along the Lorentz drift direction: $\theta_{LA} = 22.2^\circ \pm 0.1^\circ$. The second method, the *grazing angle* method, selects reconstructed tracks nearly parallel to the surface which create long clusters. The average drift distance of the electrons is measured as a function of the estimated production depth Fig. 1(c). The slope of the linear fit is $\theta_{LA} = 21.4^\circ \pm 0.6^\circ$. The two techniques agree within the errors.

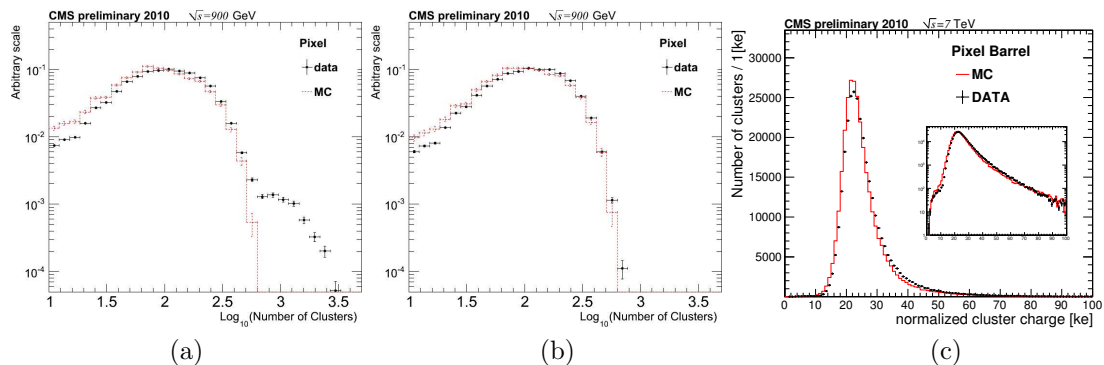


Figure 2: (a) Distribution of the number of clusters in minimum bias events; (b) distribution of the number of clusters after the background event cut; (c) normalized cluster charge in the barrel.

4 Performance with first LHC beams

The distribution of the number of clusters in minimum bias events observed with colliding beams at 900 GeV is shown in Fig 2(a), the data (dots) are compared with the simulated

events (line) [6]. A good agreement between data and MC is clear in the region with low numbers of clusters, but an excess of large multiplicity events is observed in data. Events with high occupancy have been seen since first collisions both in pixels and in strips. Typically these background events are characterized by a large number of long clusters in the barrel. Asymmetry in the r - ϕ plane suggests that the source is beam-gas interactions. A beam-gas veto, or combined cuts on the cluster shape and track quality, removes the background events as shown in Fig 2(b).

The cluster charge distribution, in the pixel barrel, normalized by the track path length to the thickness of the silicon sensor is shown in Fig 2(c), the measured distribution (dots) is in good agreement with expectation (line) [7].

The intrinsic position resolution is evaluated using tracks traversing the barrel in the overlapping regions where modules on the internal and external part of the same layer overlap by a few millimeters and are close together ($\simeq 4$ cm). The difference between the hit positions in two consecutive modules is evaluated and subtracted from the difference between the two track impact points.

The double difference is more precise than the simple difference between the extrapolated and the measured hit and moreover it is independent of the translational misalignment of the modules. Final results compared with simulation are reported in Table 1². The simulated resolutions agree reasonably well with the measured ones [7].

Data	$(12.7 \pm 2.3) \mu\text{m}$ $(28.2 \pm 1.9) \mu\text{m}$	along x along y
Simulation	$(14.1 \pm 0.5) \mu\text{m}$ $(24.1 \pm 0.5) \mu\text{m}$	along x along y

Table 1: Position resolutions.

5 Conclusion

The pixel detector has been commissioned during one year of cosmic runs. This long period of commissioning ensured that the pixel detector started data-taking with 98.3% of the modules in operation and over 99% hit efficiency. The thresholds are optimized to be sensitive up to 3200 e^- and the hit resolution is $(12.7 \pm 2.3) \mu\text{m}$ along x. The detector behaves as expected: Data and MC show a general good agreement. New data from collisions will allow further improvement in the alignment precision and calibrations. Periodical calibrations are foreseen to monitor the aging of the detector and the effects of radiation, for example, the increase of the depletion voltage and the degradation of the spatial resolution.

References

- [1] R. Adolphi *et al.* [CMS Collaboration], JINST **3** (2008) S08004.
- [2] S. Chatrchyan *et al.* [CMS Collaboration], JINST **5** (2010) T03007 [arXiv:0911.5434 [physics.ins-det]].
- [3] S. Chatrchyan *et al.* [CMS Collaboration], JINST **5**, T03009 (2010) [arXiv:0910.2505 [physics.ins-det]].
- [4] W. Erdmann [CMS Collaboration], Nucl. Instrum. Meth. A **549**, 153 (2005).
- [5] Y. Allkofer *et al.*, Nucl. Instrum. Meth. A **584**, 25 (2008) [arXiv:physics/0702092].
- [6] A. Moraes, C. Buttar and I. Dawson, Eur. Phys. J. C **50**, 435 (2007).
- [7] V. Khachatryan *et al.* [CMS Collaboration], submitted to the European Physical Journal C.

²The resolution is given both in x (r - ϕ plane) and in y (z axis); the pixel dimensions are 100 and 150 μm , respectively